J Solid State Electrochem (1998) 2: 273–280

ORIGINAL PAPER

H. Kühne · A. Fischer · T. Morgenstern · D. Grützmacher

How boron incorporation during $Si_{1-x}Ge_x$ chemical vapor deposition degrades the Ge profile

Received: 15 September 1997 / Accepted: 7 November 1997

Abstract The effect of boron incorporation during chemical vapor deposition of SiGe thin films from silane, germane, diborane, and hydrogen gas mixtures is investigated. It is shown that boron incorporation during SiGe thin-film growth degrades the Ge profile under certain growth conditions when the boron concentration is high enough ($>10^{19}$ cm^{-3}). In single-wafer atmospheric-pressure processes we find that no Ge concentration depression occurs at deposition temperatures above 675 °C. In multi-wafer atmospheric-pressure processes we find an increasingly occurring depression of the Ge concentration along the wafer stack, even at temperatures above 675 °C. In low-pressure processes, high-level in-situ doping of SiGe with boron is possible at temperatures as low as 550 °C without any degradation of the Ge profile. Thus LPCVD is superior to APCVD with respect to high-level in situ doping of SiGe with boron. The presence or absence of Ge profile degradation in boron-doped SiGe thin films is explained by the discussion of growth rate enhancement phenomena.

Key words Silicon · Germanium · CVD · Epitaxy · Boron

Introduction

Chemical vapor deposition (CVD) growth techniques cover the whole range from atmospheric-pressure (APCVD) to low-pressure (LPCVD) and even to ultra-high-vacuum conditions (VHCVD). This applies not only to silicon (Si) [1–10] but also to the growth of SiGe heterostructures [10–14].

H. Kühne (✉) · A. Fischer · T. Morgenstern
Institute for Semiconductor Physics, Walter-Korsing-Strasse 2, D-15230 Frankfurt (Oder), Germany

D. Grützmacher
Paul-Scherrer-Institut, Würenlingen und Villingen, CH-5232 Villingen PSI, Schwitzerland

In situ doping of such thin films is usually carried out with arsenic, phosphorus or boron (B), and doping levels exceeding solid solubility have been shown to be possible [15, 16]. As for the incorporation mechanism, B incorporation during silicon epitaxy for instance is controlled by way of different reaction paths, and it is the deposition condition that has actually been chosen in thin-film deposition which determines the dominant reaction mechanism. This has previously been reported in detail, showing how the actual boron incorporation mechanism for a given thin-film deposition situation can be established by investigating how the boron concentration of the film depends on the film growth rate [17]. Possible reaction paths are described as near-equilibrium, adsorption-, desorption- or reaction-controlled mechanisms. Codeposition of boron with silicon and germanium (Ge) can often be interpreted as a reaction-controlled process [18–20]. In such a case, composite layer growth is controlled by the incorporation rates of any of the layer components, I_i. The fractional atomic composition, x_i is given by the ratios of the respective partial growth rates, v_i to the total growth rate, v_L.

$$x_i = \frac{N_i}{N_L} = \frac{v_i}{v_L} \tag{1}$$

where i stands for Si, Ge and B, respectively, $N_L = \sum N_i$, N_L is the total number of atoms per cm^3 of the film, N_i that of the particular kind of element atoms considered, and $v_L = \sum v_i$.

The growth rates v, defined as the thickness increase per unit time, are related to the respective incorporation rates I (which are defined as the number of incorporated atoms per unit of area and time) and to N_L, as shown in the equation

$$v_i = \frac{I_i}{N_L}. \tag{2}$$

The incorporation rates, I_i, permit the growth rates to be related to the partial pressures of the respective source gases.

$$I_i = A_i \cdot p_{source} \quad (3)$$

where p_{source} is the partial pressure of the respective source gas and A_i is the corresponding apparent chemical reaction rate constant. In SiGeB thin film deposition, silane (SiH_4), germane (GeH_4), and diborane (B_2H_6) are commonly used as the source gases.

Real thin film heteroepitaxy is somewhat more complicated, as is expressed by Eqs. 1–3. It is characteristic of heteroepitaxial thin films that the specific density changes when the composition of the film alters. In consequence, N_L is also changed. This alteration is produced by the lattice mismatch of the codeposited element atoms. The change in N_L can be described by the following expression [18]:

$$N_L = N_A \left[\sum x_i \frac{M_i}{\rho_i}\right]^{-1} \quad (4)$$

where N_A is Avogadro's number, M_i is the molar mass, and ρ_i is the specific density of the i^{th} kind of element. It should be mentioned that Eq. 4 can be ignored for most of the SiGe films considered, even if they are doped with boron. However, when B forms an appreciable part of the film, Eq. 4 must be applied [12, 18–20].

A further special feature of thin-film heteroepitaxy is the enhancement of the silicon growth rate v_{Si} under certain deposition conditions, when GeH_4 or B_2H_6 are present in the gas phase [21, 22]. This effect can be taken into account by the definition of additional partial growth rates, $v_{Si,j}$ where j stands for Ge, and B, respectively. For the case of SiGeB thin film, Eq. 1 (the equation of growth) must therefore be extended to [18–20].

$$v_L = v_{Si} + v_{Ge} + v_B = v_{Si/Si} + (v_{Si/Ge} + v_{Ge}) + (v_{Si/B} + v_B) \quad (5)$$

where $v_{Si/Si}$ is the pure Si growth rate obtained without GeH_4 or B_2H_6 in the gas phase.

It is of advantage to correlate $v_{Si/j}$ with v_j by the introduction of the empirical factor m_j. Equation 5 now changes to [23]

$$v_L = v_{Si/Si} + (1 + m_{Ge})v_{Ge} + (1 + m_B)\, v_B. \quad (6)$$

An interaction of B with the deposition of germanium has not been taken into account in Eq. 5 or Eq. 6. However, the existence of such an interaction cannot be completely excluded, as will be shown below. In situ B doping of SiGe films is characterized by $x_B < 0.01$ in the practical cases. In consequence, v_B is very much smaller than v_{Si} and v_{Ge}. Additional Si deposition caused by the presence of B_2H_6 in the gas phase, however, may lead to such a high value of $v_{Si/B}$ that v_B cannot be neglected in Eq. 6.

In situ B doping of SiGe films is of practical use for the preparation of heterojunction bipolar transistors (HBT) having a B-doped SiGe base region [11]. In such structures, the B content can have a peak value as high as 5×10^{19} cm^{-3}; the Ge content covers the range from

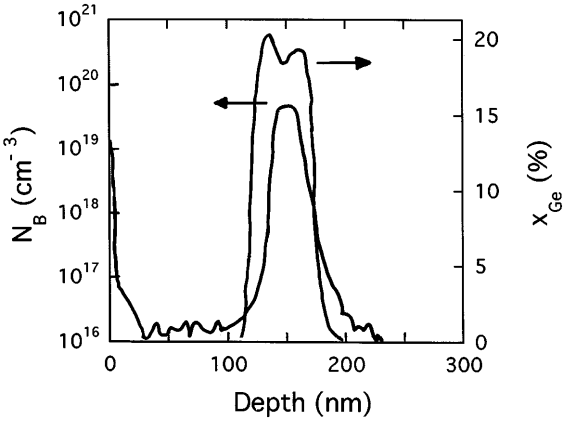

Fig. 1 SIMS profiles of B and Ge in a "box-like" device structure (B-doped SiGe base region of a hetero-bipolar transistor) as shown in [24]. Note the dip in the Ge profile within the range of B peak concentration. (APCVD; single-wafer system; $T = 550$ °C)

10 to 25%, and the base width is about 50 nm. A typical HBT base structure characterized by its B and Ge profile is shown in Fig. 1. This base region was grown with the GeH_4 and the SiH_4 input flow rates kept constant while the B_2H_6 input flow was turned on. Note the dip in the Ge profile at the B peak concentration. Si growth rate enhancement caused by the presence of B_2H_6 in the gas phase was assumed to be the origin of this Ge profile degradation [24]. Thus, additional gas flow control is needed in the careful tailoring of the intended Ge profile during the preparation of practical HBT structures.

It is the purpose of the present paper to investigate why and to what degree B incorporation degrades the Ge profile during in situ doping of SiGe films. Atmospheric-pressure (AP) and low-pressure (LP) epitaxy as well as single-wafer (SW) and multi-wafer (MW) processes are considered for those deposition conditions typical in practice. The paper will discuss how Ge profile degradation caused by in situ B doping depends on temperature and how APCVD and LPCVD influence this phenomenon. It will be shown that APCVD combined with a SW deposition system does not produce Ge profile degradation when the deposition temperature is chosen at 675 °C and above, whereas Ge profile degradation does occur in the range 550–650 °C. In the case of MW deposition systems, Ge profile degradation develops along the wafer susceptor even if deposition is carried out at 700 °C and above. This effect is produced by the different degrees of source gas exhaustion which SiH_4 and GeH_4 experience during their passage through the reaction chamber when B_2H_6 is present in the gas phase at a high enough partial pressure. As a special advantage of LPCVD, it is shown that Ge degradation does not occur even at low deposition temperatures, for instance 550 °C. In LPCVD, the B_2H_6 partial pressure which is needed to reach a preselected B doping level of the SiGe film is smaller by about two orders of magnitude than that which has to be chosen in APCVD. In such a low range of B_2H_6 content in the gas phase, en-

hancement of growth rates does not occur, and, in consequence, the Ge profile is not altered. Thus LPCVD is superior to APCVD with respect to high-level in situ doping of SiGe with boron.

The single wafer process at atmospheric pressure

In the present section, an attempt will be made to calculate how the fractional atomic Ge content, x_{Ge} of a SiGe layer depends on B_2H_6 partial pressure on the one hand and on deposition temperature on the other. The different Ge content of SiGe and SiGeB films is formally expressed as

$$x_{Ge(Si/Ge)} = \frac{N_{Ge}}{N_{L(Si/Ge)}} = \frac{v_{Ge}}{v_{L(Si/Ge)}} \quad (7a)$$

$$x_{Ge(Si/Ge/B)} = \frac{N_{Ge}}{N_{L(Si/Ge/B)}} = \frac{v_{Ge}}{v_{L(Si/Ge/B)}} \quad (7b)$$

For the calculation of $v_{L(Si/Ge/B)}$ Eq. 6 and for that of $v_{L(Si/Ge)}$ a reduced version of Eq. 6 is used. The latter reads as follows:

$$v_{L(Si/Ge)} = v_{Si/Si} + (1 + m_{Ge})v_{Ge}. \quad (6a)$$

In analogy to Eq. 6a, the growth rate of the binary SiB system can be expressed by

$$v_{L(Si/B)} = v_{Si/Si} + (1 + m_B)v_B. \quad (6b)$$

SiGeB thin films were grown using SiH_4, GeH_4, B_2H_6 as reactive gases in an H_2 atmosphere. The B_2H_6 partial pressure range considered runs from 10^{-4} to 2×10^{-1} Pa (where $p_{SiH_4} = 60$ Pa and the total gas input flow rate $\dot{V}_{tot} = 27$ l min^{-1}), the deposition temperatures cover the range from 550 to 750 °C [24]. Though the experimental basis upon which our consideration is based is small, we are able to develop a mechanism to make an unambiguous prediction of the Ge content, x_{Ge}, as it is observed with and without B_2H_6 in the gas phase. In the following, we show how figures for the quantities $v_{Si/Si}$, $v_{Si/B}$, $v_{Si/Ge}$, v_B, v_{Ge}, m_B, and m_{Ge} can be obtained. To this end, the binary SiB system is considered first. In [24], data are given on the growth rate, $v_{L(Si/B)}$, and the boron content, N_B, as a function of B_2H_6 partial pressure, $p_{B_2H_6}$ for four different temperatures. Figure 2 shows the $v_{L(Si/B)}$ values using a log scale as a function of the reciprocal temperature, and $p_{B_2H_6}$ is varied. As can be seen in Fig. 2, at $p_{B_2H_6} = 10^{-4}$ Pa the growth rate is not altered by the presence of B_2H_6 in the gas phase and $v_{L(Si/B)} = v_{Si/Si}$ is guaranteed. The growth rate shows an exponential decay below $T = 650$ °C as characterized by the linearity of the Arrhenius plot. The latter yields an apparent activation energy $E_{a_{Si}} = 1.78$ eV typical for pure Si deposition in the kinetically-controlled region of film growth. Above $T = 670$ °C, the curve gradually flattens and the slope yields $E_{a_{Si}} = 0.47$ eV at 850 °C. This is conventionally explained by assuming a transition from the kinetically to the mass-transfer controlled growth

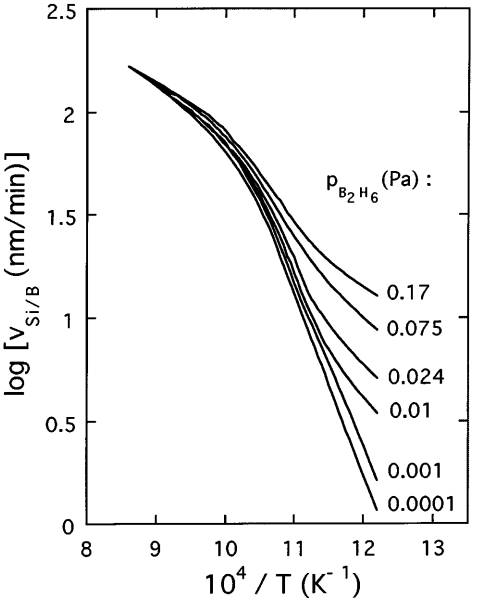

Fig. 2 Arrhenius plots of the total growth rate, $v_{L(Si/B)}$ for the binary SiB system for six different diborane partial pressures, $p_{B_2H_6}$. (Experimental data from [24]; APCVD; single-wafer system)

mechanism at higher temperatures [25]. Figure 2 shows Si deposition enhancement for the low-temperature region, when $p_{B_2H_6}$ exceeds 10^{-4} Pa. At higher temperatures Si deposition enhancement does not occur, though B_2H_6 is present in the gas phase. Interestingly, at lower deposition temperatures the growth rate increase becomes more and more evident with increasing $p_{B_2H_6}$. However, despite this increase in the deposition rate at low temperatures and high $p_{B_2H_6}$ values, N_B depends linearly on $p_{B_2H_6}$ for all deposition temperatures [24]. Consequently the partial boron growth rate, v_B, will not depend linearly on $p_{B_2H_6}$; rather it will increase superlinearly. The partial rate v_B can be obtained from the experimental data using Eq. 8, which reads as

$$v_B = v_{L(Si/B)}x_B \quad (8)$$

where $x_B = N_B/N_{L(Si/B)}$ and $N_{L(Si/B)} \approx N_{Si} = 4.995 \times 10^{22}$ cm^{-3} for $N_B < N_{Si}$; $N_{L(Si/B)} = N_{Si}$ is a suitable approximation, since $\Delta N_L/N_L < 0.02$ is confirmed even for the maximum B content of ca. 2×10^{21} cm^{-3}, as can be shown by the application of Eq. 4.

In Fig. 3, v_B is shown as a function of temperature for four selected $p_{B_2H_6}$ values. The figures illustrate how v_B depends on both temperature and $p_{B_2H_6}$. In general, as can be seen in Fig. 3, v_B decreases slightly with the decrease of temperature, but, in the case of higher $p_{B_2H_6}$ values, it starts to increase at 600 °C and below. The above-mentioned small superlinearity of v_B in the range of low temperatures and high $p_{B_2H_6}$ values is caused by the growth rate increase observed especially in the range of low temperatures and high $p_{B_2H_6}$ values (cf. Fig. 2). Nevertheless, it should be mentioned that the intention of the present paper is to discuss how B incorporation influences the Ge content of SiGe structures and not

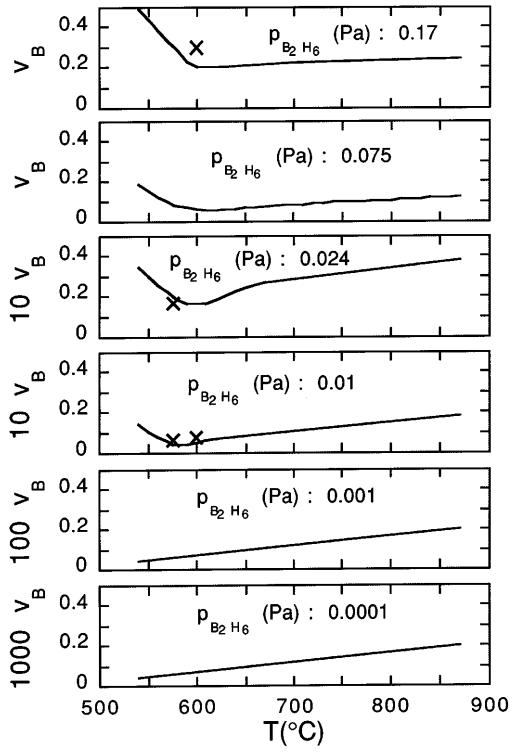

Fig. 3 The partial growth rate, v_B (measured in nm min^{-1}), for SiB deposition as a function of temperature is shown for four different diborane partial pressures, $p_{B_2H_6}$. Also shown are data for the SiGeB system represented by the cross symbols. (Original data from [24]; APCVD; single-wafer system)

how B incorporation proceeds. (For the latter, see [18–20]). The knowledge of v_B and $v_{Si/Si}$ values in addition to that of $v_{L(Si/B)}$ enables us to estimate the partial rate of additionally deposited silicon, $v_{Si/B}$, using

$$v_{Si/B} = v_{L(Si/B)} - v_{Si/Si} - v_B. \quad (9)$$

The application of Eq. 6b yields the enhancement factor m_B, which is shown in Fig. 4 as a function of $p_{B_2H_6}$

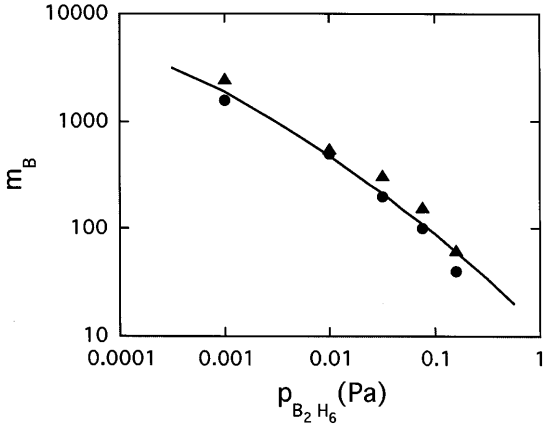

Fig. 4 The Si deposition enhancement factor m_B (defined by Eq. 6b) as a function of $p_{B_2H_6}$ for two different temperatures; (▲ 600 °C, ● 575 °C)

using the log/log scale for selected temperatures. Its values cover the range from 40 to 1500 with the higher values at the lower partial pressures. Figure 4 illustrates that m_B is more strongly a function of $p_{B_2H_6}$ than of temperature.

Let us now turn to the ternary SiGeB system, which is characterized by the additional input of the source gas GeH_4 with $p_{GeH_4} = 3.7$ Pa. In [24], data are given for $v_{L(Si/Ge/B)}$, x_{Ge}, and N_B as functions of $p_{B_2H_6}$ at two different temperatures. First we calculate v_B by the application of Eq. 8 using $v_{L(Si/Ge/B)}$ instead $v_{L(Si/Ge)}$ and $x_B = N_B/N_{Si}$. The result of our calculation is also shown in Fig. 3 and indicated by the cross symbols. The crosses illustrate that, at least for the case of deposition under consideration, v_B is not noticeably changed by the codeposition of Ge. $v_{B(Si/Ge/B)} = v_{B(Si/B)}$ is an acceptable approach. This is supported by results reported previously on B incorporation during SiGe CVD [18–20]. There it was shown that the value of the B incorporation rate $I_B = N_L v_B$ is virtually unchanged by the presence of Ge in the film up to about $x_{Ge} = 0.25$. This level is not exceeded in the films discussed here. Thus, those values which have been obtained for the binary SiB system may be used not only for $v_{Si/Si}$ but also for m_B in calculations for the ternary SiGeB system.

As for the partial growth rate, v_{Ge}, this rate is obtained from experimental data in analogy to v_B using

$$v_{Ge} = v_{L(Si/Ge/B)} \; x_{Ge}. \quad (10)$$

The results are shown in Table 1, which contains v_{Ge} as a function of $p_{B_2H_6}$ for two different temperatures. Though there is a certain rate enhancement visible for higher $p_{B_2H_6}$ values, the rate increase is only small, and, unfortunately, cannot be transmitted to deposition temperatures other than those shown. So, in the present context, we exclude the possibility of Ge growth rate enhancement by the presence of B_2H_6 in the gas phase and take the average values as the basis of our further considerations. Extrapolation to other deposition temperatures is done by taking into account the given temperature dependence, which leads to the empirical equation given below

$$\log v_{Ge} = 0.5119 - 0.5655 \left(\frac{10^4}{T} - 11.79\right), \quad (11)$$

where $0.5119 \equiv \log 3.25 \equiv \bar{v}_{Ge}$ at $T = 575$ °C, i.e. $10^4/T = 11.79$ K^{-1}, and $0.5655 = \Delta \log v_{Ge}/\Delta(10^4/T)$.

Table 1 Dependence of v_{Ge} on T and $p_{B_2H_6}$

v_{Ge} (nm/min)		$p_{B_2H_6}$(Pa)
At 575 °C	At 600 °C	
–	4,8	$2{,}7 \cdot 10^{-4}$
2,9	4,8	$1 \cdot 10^{-2}$
3,6	–	$2{,}7 \cdot 10^{-2}$
–	5,3	$1{,}7 \cdot 10^{-1}$

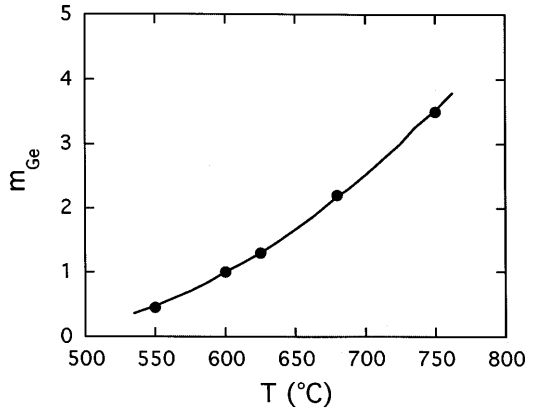

Fig. 5 The Si deposition enhancement factor m_{Ge} (defined by Eq. 6b) as a function of temperature. (Data from [27, 28])

Equation 11 yields $E_{a_{Ge}} = 1.13$ eV; this value matches perfectly that given by Kim and co-workers [24] for $x_{Ge} = 0.16$ and 0.31.

The Ge-related factor of Si deposition enhancement, m_{Ge} is taken from [27, 28], and its dependence on temperature is shown in Fig. 5. Now we are able to estimate the values of both $v_{L(Si/Ge)}$ and $v_{L(Si/Ge/B)}$ for the whole temperature range. Using Eq. 7b, we can discuss how x_{Ge} changes when the B_2H_6 partial pressure is systematically varied. Figure 6 shows x_{Ge} as a function of temperature in the range from 550 to 750 °C for three different $p_{B_2H_6}$ values. The symbols in Fig. 6 indicate the $x_{Ge(Si/Ge/B)}$ values which are reported in [24]. These values correspond well with the calculated curves and, therefore, confirm our calculation. The upper curve in Fig. 6 shows the course of x_{Ge} for the binary Si/Ge system. Boron does not influence the total growth rate at $p_{B_2H_6} \leq 10^{-4}$ Pa, as has already been mentioned above. In consequence, x_{Ge} is not changed by in situ doping with boron at such a low level. The middle curve clearly shows a lower increase of x_{Ge} with decreasing temperature within the temperature range below 675 °C; this effect is caused by the B_2H_6 partial pressure increase to $p_{B_2H_6} = 10^{-2}$ Pa. A further increase of $p_{B_2H_6}$ to about $p_{B_2H_6} = 2 \times 10^{-1}$ Pa even produces a decrease of x_{Ge} in the temperature range below 650 °C.

Our consideration above leads to the conclusion that SW processing in APCVD does not degrade the Ge profile during SiGe thin-film growth when high-level boron doping (ca. 5×10^{19} cm^{-3}) is carried out at deposition temperatures above 675 °C. The Ge profile degradation which has been observed at temperatures below 675 °C is caused by Si deposition enhancement in the presence of B_2H_6 when the latter is present in the gas phase at a high enough level.

The multi-wafer process at atmospheric pressure

In contrast to the conclusion stated above, considerable degradation of the Ge profile has been observed in MW APCVD at 725 °C. Deposition was carried out from a SiH_4, GeH_4, B_2H_6, H_2 and hydrogen chloride (HCl) gas mixture using a horizontally arranged, inductively heated graphite cuboid as the susceptor. The degradation observed is illustrated in Fig. 7, which relates to the penultimate position of a susceptor suitable for five 4″ wafers. The figure shows the Ge and B profiles of a sample, the first layer of which, d_1, was SiGe, followed by a B-doped SiGe layer, d_2, with a considerably degraded Ge content in comparison with the first layer. The third layer, d_3, was again deposited as pure SiGe after the B_2H_6 input flow was stopped. A small difference is also visible in the Ge content of the first and

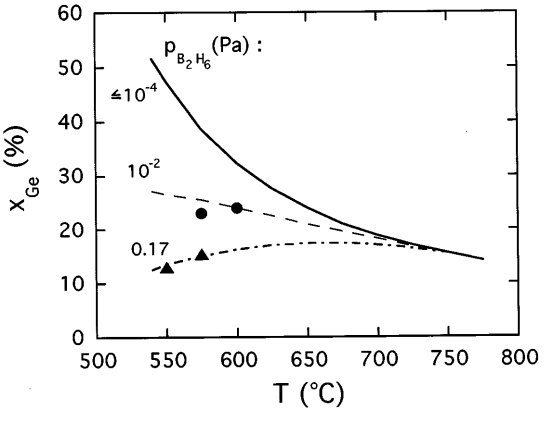

Fig. 6 The calculated fractional atomic Ge content, x_{Ge}, of SiGeB thin films (deposition condition as shown in [24]; APCVD; single-wafer system) as a function of temperature for three different $p_{B_2H_6}$ values: $p_{B_2H_6} \leq 10^{-4}$ Pa represents the behavior of B-free and weakly B-doped SiGe films; $p_{B_2H_6} = 10^{-2}$ Pa and $p_{B_2H_6} = 1.7 \times 10^{-1}$ Pa show the increasing depression of x_{Ge} due to B_2H_6-induced Si deposition enhancement, which effect arises above all in the range of growth temperatures below 675 °C

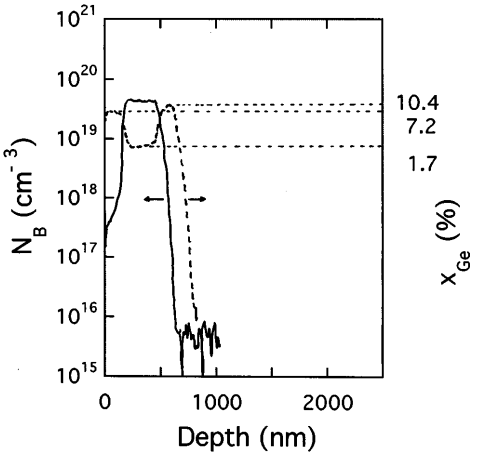

Fig. 7 SIMS profiles of B and Ge for a SiGe/SiGeB/SiGe-sandwiched thin film with a clear indication of Ge profile depression due to B doping within the middle layer. (APCVD; multi-wafer system; deposition from SiH_4, GeH_4, HCl, H_2, and (for a certain time) B_2H_6 gaseous mixture. The profiles shown belong to the penultimate wafer of five 4″ wafers arranged flat and one behind the other in the direction of the gas flow; $T = 725$ °C)

third layers. This difference can be explained as the result of an unintended gradual increase of temperature during the deposition process, which lasted about 60 min. To average this temperature effect, the Ge contents of the first and third layers are represented by the arithmetic mean value obtained from them. The relative Ge profile degradation caused by B doping of SiGe is then given as

$$\frac{N_{\mathrm{Ge(Si/Ge/B)}}}{N_{\mathrm{Ge(Si/Ge)}}} = \frac{2\,x_{\mathrm{Ge}_2}}{x_{\mathrm{Ge}_1} + x_{\mathrm{Ge}_3}} \tag{12}$$

This degradation, as defined by Eq. 12, is shown in Fig. 8 as a function of the wafer position on the susceptor. The figure shows degradation to be developed along the susceptor. It is imperceptibly small at the beginning. The latter observation corresponds with our findings in connection with the SW process. In contrast to the conditions of thin film growth selected in the SW process, MW deposition was carried out at 725 °C, $p_{\mathrm{SiH_4}} = 58$ Pa, $p_{\mathrm{GeH_4}} = 33$ Pa, $p_{\mathrm{B_2H_6}} = 1.1$ Pa, $p_{\mathrm{HCl}} = 149$ Pa, and $\dot{V}_{\mathrm{H_2}} = 27.5$ l min^{-1}. Note that the content of B_2H_6 in the gas phase had to be increased drastically because of the presence of HCl [29]. Naturally not only the B incorporation rate is reduced by HCl but also the partial growth rates of Si and Ge [30].

The total thickness, d_{L}, of any of the separate layers was evaluated by splitting them into the Si deposition and Ge deposition part using Eq. 13a and b to estimate d_{Ge} and d_{Si}, respectively

$$d_{\mathrm{Ge}} = d_{\mathrm{L}} x_{\mathrm{Ge}}, \tag{13a}$$

$$d_{\mathrm{Si}} = d_{\mathrm{L}} - d_{\mathrm{Ge}} = d_{\mathrm{L}}(1 - x_{\mathrm{Ge}}). \tag{13b}$$

The thicknesses of the separate layers were measured precisely by the application of cross-section TEM [G. Morgenstern (1995) unpublished research].

Note that the partial thicknesses stand for the respective growth rates, for each of the separate layers of the sandwiches was deposited during a preselected, constant period of time (20 min). Figure 9 shows how $v_{\mathrm{Si}}/v_{\mathrm{Ge}}$ develops along the susceptor for each of the three separate layers. Though the absolute growth rates, represented by the separate layer thicknesses, decrease along the susceptor, the ratio $v_{\mathrm{Si}}/v_{\mathrm{Ge}}$ remains virtually unchanged for the undoped SiGe layers 1 and 3. This means that the degree of source gas depletion along the susceptor, which occurs as a result of Si and Ge deposition, is nearly equal for SiH_4 and GeH_4. In contrast to this, $v_{\mathrm{Si}}/v_{\mathrm{Ge}}$ strongly increases along the susceptor when the layer contains boron to a sufficient degree, as is the case for the middle layer of the sandwich (layer 2). This could be understood if Si deposition were increasingly enhanced along the susceptor. Consequently, a reduction of x_{Ge} should be observed even at the beginning of the susceptor. However, this is indicated neither in Fig. 8 nor in Fig. 9. So we have to assume that the action of B_2H_6 causes not only Si but also Ge deposition enhancement. In Fig. 10 the partial Si and Ge growth rates of the three separate layers 1–3 were drawn against

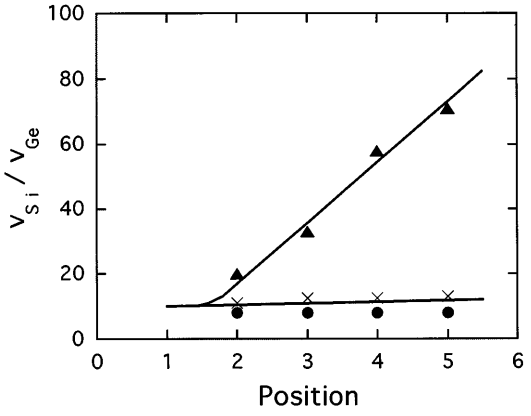

Fig. 9 The growth rate ratio, $v_{\mathrm{Si}}/v_{\mathrm{Ge}}$ is shown for each separate layer of the SiGe/SiGeB/SiGe-sandwiched thin film as a function of the wafer position on the susceptor: ● $(v_{\mathrm{Si}}/v_{\mathrm{Ge}})_1$; ▲ $(v_{\mathrm{Si}}/v_{\mathrm{Ge}})_2$; × $(v_{\mathrm{Si}}/v_{\mathrm{Ge}})_3$. (Details as in Figs. 7 and 8)

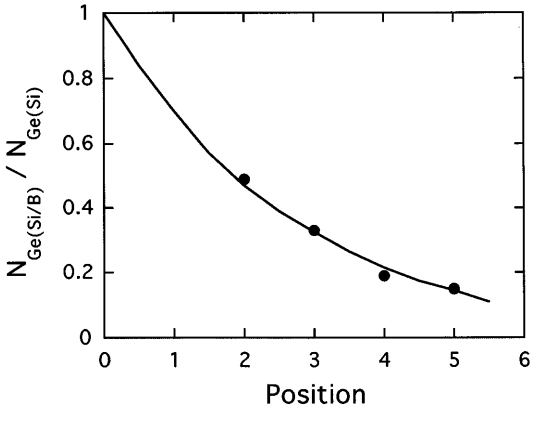

Fig. 8 The relative Ge content depression, $2\,x_{\mathrm{Ge}_2}/(x_{\mathrm{Ge}_1} + x_{\mathrm{Ge}_3})$ as caused by B doping of SiGe is shown as a function of the wafer position on the susceptor. (Gas flow from left to right; the wafer position number marks the center of the corresponding wafer; details as in Fig. 7)

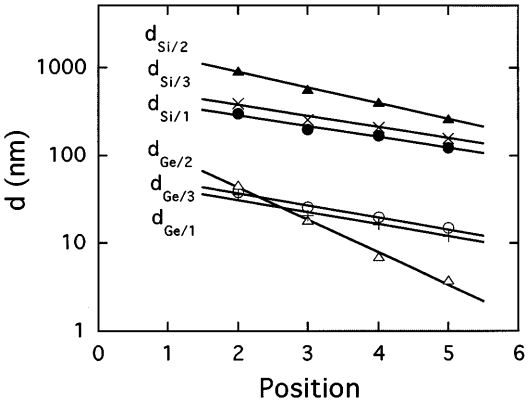

Fig. 10 The partial layer thicknesses d_{Si} and d_{Ge} (which quantities stand for the growth rates) are shown using the log-normal scale for each separate layer of the SiGe/SiGeB/SiGe-sandwiched thin film as a function of the wafer position on the susceptor. (Details as in Figs. 7 and 8)

the wafer position using the log-normal scale. The linear courses of the curves correspond to the exponential growth rate distribution along the susceptor [31] as shown in the equation

$$v(x) = v(0) \exp -B_i x \tag{14}$$

where $v(x)$ is the growth rate at position x and $v(0)$ that at $x = 0$, B_i is a theoretically based constant, and x indicates the position along the susceptor. The exponential growth rate distribution clearly indicates the linear relation between growth rate and the partial pressure of the respective source gas [31], as is demonstrated by

$$v(0) = \frac{A_i}{N_L} p_{source}(0) \tag{15}$$

where $p_{source}(0)$ is the source gas partial pressure at $x = 0$ for which the input partial pressure is conventionally taken.

In Fig. 10 the undoped separate SiGe layers 1 and 3 show an almost parallel decrease for the partial growth rate of both Si (upper curves) and Ge (lower curves). The B-doped layer 2 indicates a considerably enhanced growth rate for Si as well as Ge. The latter observation reveals a surprising fact, which had hitherto not been taken into consideration in discussions about growth rate enhancement as caused by the presence of B_2H_6 in the gas phase. The rate $v_{Si/2}$ is greater than $v_{Si/1}$ and $v_{Si/3}$ at any position of the susceptor. From this we conclude that the additional consumption of SiH_4 caused by the enhanced deposition rate at the beginning of the susceptor is fully counterbalanced by a higher degree of SiH_4 conversion during the gas passage through the deposition chamber [31, 32]. Thus, the presence of B_2H_6 in the gas phase causes not only A_i in Eq. 15 but also B_i in Eq. 14 to change. The rate $v_{Ge/2}$ is greater than $v_{Ge/1}$ and $v_{Ge/3}$ in the entry part of the susceptor but falls below $v_{Ge/1}$ and $v_{Ge/3}$ from the third wafer position to the end of the susceptor. In contrast to Si deposition, the additional GeH_4 consumption at the beginning of the susceptor caused by $v_{Ge/2}$ enhancement in the case of B-doped SiGe growth is not or only partly counterbalanced by a higher degree of GeH_4 conversion during the gas passage through the deposition chamber. In the case of Ge deposition, B_2H_6 causes A_i to change rather than B_i in Eqs. 15 and 14 respectively. As a consequence of the enhanced GeH_4 consumption at the beginning of the deposition zone during high-level B doping of SiGe thin film, which leads to enhanced depletion effects, and the almost total lack of enhanced SiH_4 depletion effects in such a case, the Ge content of B-doped SiGe thin films becomes smaller and smaller along the susceptor.

Our experimental findings and theoretical considerations above lead to the conclusion that MW processing in APCVD develops increasing Ge profile degradation along the susceptor even when high-level B doping is carried out at deposition temperatures above 675 °C. The Ge profile degradation observed is caused by the increased depletion of GeH_4 in the gas phase during the GeH_4 passage through the deposition zone. This increased depletion is caused by Ge deposition enhancement in the presence of B_2H_6 in the gas phase. Thus, B_2H_6 enhances the growth rate of both Si and Ge, but does not enhance the degree of GeH_4 conversion into Ge in contrast to that of SiH_4 into Si.

The low-pressure process

APCVD has recently seen a revival with SiGe epitaxy. But, apart from this, LPCVD processes are more convenient in micro-electronic technologies. They ensure a broader technological window with respect to Si epitaxy for both low-temperature application and selective growth. Nevertheless, LPCVD is also of particular advantage for SiGe epitaxy. No Ge profile degradation is observed during the 5×10^{19} cm^{-3} B in situ doping of SiGe. This is shown in Fig. 11 by the example of an SiGe/SiGeB/SiGe sandwiched thin-film structure deposited at $p_{total} = 200$ Pa and $T = 550$ °C from an SiH_4, GeH_4, H_2 mixture within a single-wafer deposition reactor. B_2H_6 was temporarily added to the gas phase [B. Tillack (1996) unpublished research].

It is known that v_{Si} decreases when p_{H_2} is increased in Si CVD. In contrast, v_{Si} increases when LPCVD conditions are chosen where p_{H_2} is decreased. However, attention has hitherto been focused less on the fact that a certain doping level desired in Si epitaxy can be reached with a much lower dopant source content in the gas phase at LP than under AP conditions. Nevertheless, this had already been shown in 1982 for arsenic and phosphorus as the doping elements [33]. The reference cited illustrates that the arsenic content of an Si film which was grown at 1080 °C from a hydrogen atmosphere increases from 10^{16} to 10^{17} cm^{-3} when, at constant arsine partial pressure, the hydrogen partial pressure is decreased from atmospheric pressure to

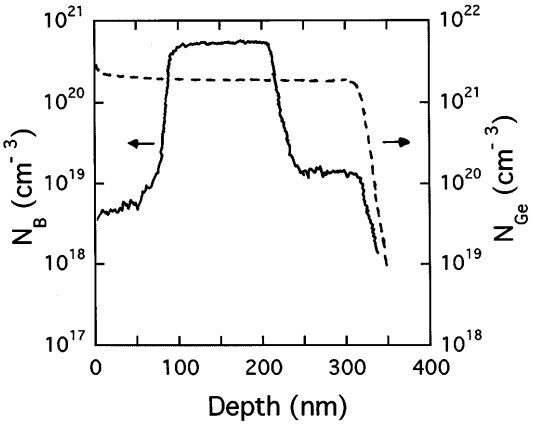

Fig. 11 SIMS profiles of B and Ge for a SiGe/SiGeB/SiGe-sandwiched thin film showing no Ge profile degradation. (LPCVD single-wafer system; deposition from SiH_4, GeH_4, H_2, and (for a certain time) B_2H_6; total pressure, $p_{tot} = 200$ Pa; $T = 550$ °C)

5.4×10^3 Pa. In the case of phosphorus doping, on the other hand, $N_P = 10^{16}$ cm^{-3} can be reached at reduced pressure ($p_{total} = 10^4$ Pa) with a quarter of the phosphine input rate than is needed at atmospheric pressure.

The increase of the doping level at constant partial pressure of the dopant source gas with a decrease in total pressure is as typical for boron as for arsenic or phosphorus. The SiGe sample shown in Fig. 11 contains in its middle part $N_B = 5 \times 10^{19}$ cm^{-3}; this doping level was reached by the application of $p_{B_2H_6} = 1.7 \times 10^{-4}$ Pa. In SW APCVD SiGe epitaxy at 575–600 °C, this doping level needs the application of $p_{B_2H_6} = 2.3 \times 10^{-2}$ Pa and at 725 °C with 149 Pa of HCl in the gas phase even as much as $p_{B_2H_6} = 1.1$ Pa. In SiGe LPCVD, the partial pressure applied is at least two orders of magnitude smaller than that needed in SiGe APCVD to achieve the same doping level. In the range of $p_{B_2H_6} = 10^{-4}$ Pa, however, there is no effect of boron present in the gas phase on the film growth rate at all. The lack of Si growth rate enhancement, though B_2H_6 is present, also means that there is no reduction in the Ge content of the film. In the end, LPCVD proves itself superior to APCVD with respect to high-level in situ doping of SiGe with boron.

Summary and conclusions

We have investigated how B incorporation during CVD of SiGe degrades the Ge content of the film. It has been shown that all the observed phenomena can be understood as being caused by the presence or lack of growth rate enhancement due to the presence of B_2H_6 in the gas phase at a high or low enough level.

In SW APCVD processes, the Ge concentration of the deposited films is not reduced, though high-level B doping takes place, when the deposition temperature is higher than 675 °C. This is explained by the way in which growth rate enhancement due to the action of B_2H_6 depends on both temperature and B_2H_6 partial pressure.

In MW APCVD processes, the Ge concentration depression is progressively reduced along the wafer stack, even if $T > 675$ °C is chosen. This is understood as the result of both the increase of SiH_4 conversion efficiency due to the action of B_2H_6 and the deposition enhancement of Si and Ge, also caused by B_2H_6. Both effects lead to an increasing depletion effect for GeH_4, along the wafer stack, in comparison to SiH_4.

In LPCVD processes, high-level in situ B doping of SiGe is possible at temperatures as low as 550 °C without any degradation of the Ge content of the film. This is because the partial pressure value needed for high-level doping is less by several orders of magnitude than the value needed at atmospheric pressure. Such low values are uncritical with respect to pressure values at which growth rate deposition enhancement occurs.

We therefore conclude that LPCVD is superior to APCVD with respect to high-level in situ doping of SiGe with boron.

References

1. Bloem J, Gilling LJ (1978) In: Kaldis E (ed) Current topics in materials science, vol I. North-Holland, Amsterdam
2. Schneider HG, Ickert L (1984) Halbleiterepitaxie. Akad Verl Gesellschaft Geest & Portig, Leipzig
3. Comfort JH, Reif R (1989) J Electrochem Soc 136: 2386
4. Murota J, Takasawa Y, Fujimoto H, Goto K, Massura T, Sawada Y (1995) J de Phys IV colloque C5, Suppl II 5: C5-1165
5. Gates SM, Kulkarni SK (1991) Appl Phys Lett 58: 2963
6. Liehr M, Greenlief CM, Kasi SR, Offenberg M (1990) Appl Phys Lett 56: 629
7. Dutartre D, Warren P, Berbezier I, Perret P (1992) Thin Sol Films 222: 52
8. Gates SM (1992) J Cryst Growth 120: 269
9. Meyerson BS, Himpel FJ, Uram KJ (1990) Appl Phys Lett 57: 1034
10. Meyerson BS (1990) JBMJ Res Develop 34: 806
11. Greve DW (1993) Materials Sci Eng B 18: 22
12. Murase K (1991) J Mat Res 6: 92
13. Dutartre D, Warren P, Provenier F, Chollet F, Dério A (1994) J Vac Sci Technol A12 (4): 1009
14. Greve DW, Misra R, Strong R, Schlesinger TE (1994)
15. Meyerson BS, Le Groues FK, Nguygen TN, Harame DL (1987) Appl Phys Lett 50: 113
16. Hellberg P-E, Gagnor A, Thang S-L, Petersson CS (1997) J Eletrochem Soc in press
17. Kühne H, Fischer A, Öztürk MC, Sanganeria K (1996) J Eletrochem Soc 143: 634
18. Kühne H, Fischer A (1995) Semicond Sci Technol 9: 1666
19. Kühne H, Fischer A (1995) Semicond Sci Technol 9: 1833
20. Kühne H, Fischer A (1995) Semicond Sci Technol 10: 846
21. Eversteyn FC, Put BH (1973) J Electrochem Soc 120: 106
22. Kamins Ti, Meyer DJ (1991) Appl Phys Lett 58: 178
23. Kühne H (1993) Appl Phys Lett 62: 1967
24. Sedgwick To, Grützmacher DA (1995) J Electrochem Soc 142: 2458
25. Eversteyn FC, Peek HL (1970) Philips Res Repts 25: 472
26. Kim JW, Ruyn M-K, Kim K-B, Kim S-J (1996) J Electrochem Soc 143: 363
27. Kühne H, Richter H (1993) J Cryst Growth 129: 321
28. Kühne H, Richter H (1996) J Cryst Growth 132: 357
29. Morgenstern T, Kühne H, Kokowin GA, Testova NA, Titov AA (1987) Cryst Res Technol 22: 75
30. Kühne H, Kissinger G, Zaumseil P, Hinrich S, Richter H (1993) Mat Res Soc Proc 280: 183
31. Kühne H (1993) Cryst Res Technol 28: 39
32. Kühne H (1995) Cryst Res Technol 30: 317
33. Kühne H (1982) Cryst Res Technol 17: 181